DISCLAIMER

This report was prepared as an account of work sponsored by an agency of the United States Government. Neither the United States Government nor any agency thereof, nor any of their employees, makes any warranty, express or implied, or assumes any legal liability or responsibility for the accuracy, completeness, or usefulness of any information, apparatus, product, or process disclosed, or represents that its use would not infringe privately owned rights. Reference herein to any specific commercial product, process, or service by trade name, trademark, manufacturer, or otherwise does not necessarily constitute or imply its endorsement, recommendation, or favoring by the United States Government or any agency thereof. The views and opinions of authors expressed herein do not necessarily state or reflect those of the United States Government or any agency thereof. Reference herein to any social initiative (including but not limited to Diversity, Equity, and Inclusion (DEI); Community Benefits Plans (CBP); Justice 40; etc.) is made by the Author independent of any current requirement by the United States Government and does not constitute or imply endorsement, recommendation, or support by the United States Government or any agency thereof.

ANL/CFCT-25/22

Property Measurements of LiF-NaF-KF Molten Salts Doped with Corrosion Products and Oxygen

Chemical and Fuel Cycle Technologies Division

ANL/CFCT-25/22

Property Measurements of LiF-NaF-KF Molten Salts Doped with Corrosion Products and Oxygen

prepared by
L.D. Gardner, E.A. Dowding, J. Rojas, and M.A. Rose
Chemical and Fuel Cycle Technologies Division, Argonne National Laboratory

September 30, 2025

ACKNOWLEDGEMENTS

This report was produced under the auspices of the US DOE Advanced Reactor Technology Program Molten Salt Reactor Campaign. Issuance of this report meets milestone M3AT-25AN0705014. The authors gratefully acknowledge efforts by Ms. Kristin DeAngeles, Ms. Susan Lopykinski, Dr. Seema Naik, and Ms. Yifen Tsai (Argonne Analytical Chemistry Laboratory) for compositional analyses of salt samples. This work was conducted at Argonne National Laboratory and supported by the U.S. Department of Energy, Office of Nuclear Energy, under Contract DE-AC02-06CH11357.

CONTENTS

LIST OF TABLES

LIST OF FIGURES

1. Introduction

Measurements of thermophysical properties of molten salts are needed for modeling and simulation activities that support the development of molten salt reactor (MSR) technologies. Properties of interest including transition temperatures, phase behavior, heat capacity, density, volumetric thermal expansion, surface tension, viscosity, thermal diffusivity, thermal conductivity, and vapor pressure are being performed at Argonne [1–2]. Results of these property measurements are suitable for use in evaluating reactor performance during startup and the early operating life of the reactor.

Ingressions of oxygen and moisture into the fuel salt are expected to occur at different times during the operating life of the reactor due to system leaks, maintenance, and refueling activities. The presence of these environmental contaminants induces corrosion of structural materials. The introduction of corrosion-derived species, oxygen and moisture is expected to affect the physical and chemical properties of the salt and operation of the reactor. Previous work performed at Argonne evaluated the effects of fission product dopants on the thermal properties of eutectic LiF-NaF-KF (FLiNaK) [1–2]. Properties of FLiNaK are commonly used to represent those of fluoride-bearing fuel salts. Metallic corrosion products such as chromium and nickel ions together with dissolved oxygen are expected to affect system redox differently than the accumulation of fission products. Work summarized in this report was performed to measure the effects of corrosion products and dissolved oxygen on the phase transitions, and specific heat capacity of FLiNaK.

Thermophysical property measurements were made using four salts that were prepared by doping aliquots of a eutectic mixture of FLiNaK with surrogate corrosion products. Controlled additions of CrF_3 and NiF_2 were used as surrogates for corrosion product contamination anticipated during extended reactor operations in which fuel salt is in contact with steel reactor components. Controlled additions of UF_4 from two sources containing known amounts of UO_2 at different concentrations were used to represent oxygen contamination. The phase transitions and specific heat capacities of the four salts were measured by using differential scanning calorimetry. Measurements were made at temperatures spanning the range of 500–900 °C, which is the expected operating range of MSRs. Measured property values were compared to values measured previously with eutectic FLiNaK without dopants. Differences between property values measured for the doped and non-doped salts were compared with the uncertainties of the measurements to determine the significance of the effect of corrosion products and oxygen on salt properties.

2. Salt Preparation and Analysis

All reagents used in the synthesis of eutectic FLiNaK and the added CrF_3 and NiF_2 had purities of ≥99%. The UF_4 used in this study was shown to contain an appreciable amount of dissolved oxygen (on the order of 1-2 wt %) present as UO_2, as confirmed by XRD and inert gas fusion analysis in previous work. A portion of this UF_4 had been previously chemically purified by reaction with NH_4HF_2 to decrease the dissolved oxygen concentration in the salt. These two sources of UF_4 having

different dissolved oxygen contents (6.32 to 3.52 wt % UO_2) were used to prepare two FLiNaK salt mixtures with different oxygen contents.

The preparation of salt mixtures and measurement samples was performed within an ultra-high purity argon atmosphere glovebox maintained with <10 ppm O_2 and <1 ppm H_2O. Salt reagents were individually heated in nickel crucibles to remove absorbed water and volatile impurities. The NaF, KF, LiF, and CrF_3 reagents were heated at 300 °C for at least four hours and then at 700 °C for at least eight hours. Reagent NiF_2 was dried at 300 °C for at least eight hours . Nickel crucibles used in salt preparation were cleaned with steel wool, methanol, and lint-free wipes to remove surface contaminants. Crucibles were baked out at 700 °C for at least four hours prior to use.

A 125-g batch of eutectic FLiNaK was synthesized for use in the preparation of doped salt mixtures. Known amounts of dried LiF, NaF, and KF were weighed, added to a nickel crucible, and fused within a Kerr furnace at 700 °C for at least eight hours. The fused ingot of salt was then removed from the cooled furnace, crushed with a clean stainless steel mortar and pestle, reloaded into the nickel crucible, and reheated. This process was repeated until the FLiNaK base salt mixture was fused and crushed three times.

Four doped salt mixtures were used in property measurements. Aliquots of eutectic FLiNaK were each doped with one of CrF_3, NiF_2, and two sources of UF_4 containing different concentrations of dissolved oxygen from before and after chemical purification. Those salt mixtures are referred to as FLiNaK-CrF_3, FLiNaK-NiF_2, FLiNaK-UF_4-A, and FLiNaK-UF_4-B, where designations A and B refer to as-received and purified UF_4, respectively. The doped salt mixtures were prepared by performing three cycles of heating at 700 °C for at least eight hours and crushing the cooled salt with a mortar and pestle. The doped salts were used for thermophysical property measurements. Measurements of doped salts will be compared to previous measurements of a batch of FLiNaK provided to Argonne as part of an inter-laboratory salt study.

The concentrations of major constituents in doped FLiNaK salt mixtures were measured by using inductively coupled plasma-optical emission spectroscopy (ICP-OES) and concentrations of trace metals were determined by using inductively coupled plasma-mass spectrometry (ICP-MS). The ICP-OES measurements were performed by using a PerkinElmer® Optima™ 8300DV ICP optical emission spectrometer, and ICP-MS measurements were performed by using a PerkinElmer® NexION® 2000 ICP mass spectrometer. Instrument calibrations were performed with standards prepared from NIST-traceable solutions.

Three samples of each salt mixture were prepared for compositional analyses. A known amount of each salt sample was dissolved in a mixture of deionized water, HNO_3, and HCl and heated overnight within a stainless steel Parr vessel at 140 °C. The concentrations of major constituents previously measured in the FLiNaK provided under an inter-laboratory study and in the doped salt mixtures, FLiNaK-CrF_3, FLiNaK-NiF_2, FLiNaK-UF_4-A, and FLiNaK-UF_4-B are shown in Tables 1–5, respectively. The concentrations were calculated by using measured cation concentrations of different

samples. Averages and one standard deviation (1 s) of the salt composition are also reported. Concentration measurements performed by ICP-MS are typically accurate to within 10% of measured values.

Table 1. Composition of major components in FLiNaK provided under the interlaboratory salt study as previously measured in ANL/CFCT-23/23, in wt %

Sample	LiF	KF	NaF
1	30.4	57.5	12.0
2	30.6	57.7	11.7
3	30.3	57.8	11.9
Average	30.4	57.6	11.9
1 s	0.1	0.3	0.2

Table 2. Composition of major components in FLiNaK-CrF_3 calculated from measured cation concentrations, in wt %

Sample No.	LiF	KF	NaF	CrF_3
1	28.0	54.7	10.9	0.80
2	29.0	53.9	11.3	1.02
3	29.0	55.0	11.2	0.92
Average	28.7	54.5	11.1	0.91
1 s	0.6	0.5	0.2	0.1

Table 3. Composition of major components in FLiNaK-NiF_2 calculated from measured cation concentrations, in wt %

Sample No.	LiF	KF	NaF	NiF_2
1	28.7	53.2	11.0	0.92
2	30.0	55.4	11.4	0.90
3	28.5	53.0	10.8	0.81
Average	29.0	53.8	11.0	0.88
1 s	0.8	1.3	0.3	0.06

Table 4. Composition of major components in FLiNaK-UF_4-A calculated from measured cation concentrations, in wt %

Sample No.	LiF	KF	NaF	UF_4
1	25.8	49.1	9.8	11.7
2	25.9	48.0	9.8	12.4
3	25.1	47.1	9.6	12.0
Average	25.6	48.1	9.7	12.0
1 s	0.5	1.0	0.1	0.4

Table 5. Composition of major components in FLiNaK-UF_4-B calculated from measured cation concentrations, in wt %

Sample No.	LiF	KF	NaF	UF_4
1	25.6	46.6	9.7	11.9
2	24.7	48.1	9.7	12.4
3	26.1	47.2	9.8	12.1
Average	25.5	47.3	9.7	12.1
1 s	0.7	0.8	0.1	0.3

The measured concentrations of trace elements in samples of doped salt mixtures FLiNaK-CrF_3, FLiNaK-NiF_2, FLiNaK-UF_4-A, and FLiNaK-UF_4-B are shown in Tables 7–10, respectively. For comparison the concentrations of trace elements in the previously measured FLiNaK salt provided under the inter-laboratory salt study are shown in Table 6. The averages and 1s values of concentrations measured in three samples are also included. In cases where impurities were not detected, the limit of detection is reported. Concentration measurements performed by ICP-MS are typically accurate to within 10% of measured values. Detectable amounts of chromium and nickel impurities were likely introduced during the crushing, drying, or fusion of salt mixtures. Elevated quantities of iron in FLiNaK-UF_4-B relative to FLiNaK-UF_4-A may be attributed to additional heating during chemical purification of UF_4. Elevated quantities of nickel in both FLiNaK-UF_4-A and FLiNaK-UF_4-B relative to the other salt mixtures may have been present in the reagent UF_4. Detectable amounts of aluminum in FLiNaK-CrF_3 may have been present as an impurity in reagent CrF_3.

Table 6. Concentrations of trace elements in FLiNaK provided by inter-laboratory salt study as measured in ANL/CFCT-23/23, in ppm

Sample No.	Cr	Ni
1	5.01	8.73
2	3.35	7.55
3	3.64	8.07
Average	4.0	8.1
1 s	0.9	0.6

Table 7. Concentrations of trace elements in FLiNaK-CrF_3, in ppm

Sample No.	Al	Ni
1	67.8	180
2	90.1	215
3	70.3	290
Average	76.1	228
1 s	12.2	56

Table 8. Concentrations of trace elements in FLiNaK-NiF_2, in ppm

Sample No.	Al*	Cr*
1	3790	9.9
2	<14.3	4.5
3	<13.6	<1.3
Average	—	7.2
1 s	—	—

*< indicates the concentration was below the reported detection limit.

Table 9. Concentrations of trace elements in FLiNaK-UF_4-A, in ppm

Sample No.	Al*	Cr	Ni
1	<14.2	18.9	3460
2	<12.6	6.0	2510
3	<14.2	7.0	1470
Average	—	10.6	2480
1 s	—	7.2	996

*< indicates the concentration was below the reported detection limit.

Table 10. Concentrations of trace elements in FLiNaK-UF_4-B, in ppm

Sample No.	Al*	Cr	Fe	Ni
1	<15.0	76.7	331	1930
2	<14.9	82.5	344	2580
3	<16.9	100	1010	2550
Average	—	86.4	562	2360
1 s	—	12.1	389	368

*< indicates the concentration was below the reported detection limit.

The concentration of dissolved oxygen in FLiNaK-UF_4-A and FLiNaK-UF_4-B were measured by using inert gas fusion analysis. Measurements were performed by using an 836 Oxygen/Nitrogen Analyzer (LECO Corporation, St. Joseph, MI). Dissolved oxygen concentrations that were measured in five 50-mg samples of each salt mixture, including averages and one standard deviation for the replicate analyses, are shown in Table 11. The inert gas fusion technique is typically accurate to within 25% of the total amount of oxygen present in the sample. The difference in average oxygen concentration between samples of FLiNaK-UF_4-A (0.75 wt. % oxygen, 6.32 equivalent wt. % UO_2) and FLiNaK-UF_4-B (0.42 wt. % oxygen, 3.52 equivalent wt. % UO_2) is attributed to the chemical purification performed on the source UF_4 used to dope FLiNaK-UF_4-B.

Table 11. Concentrations of dissolved oxygen in FLiNaK-UF_4-A and FLiNaK-UF_4-B salts, in wt. % oxygen

Sample No.	FLiNaK-UF_4-A	FLiNaK-UF_4-B
1	1.02	0.45
2	0.90	0.42
3	0.69	0.39
4	0.58	0.38
5	0.56	0.45
Average	0.75	0.42
1 s	0.20	0.04

3. Melting Temperature

3.1 Method

Thermal analyses of doped-FLiNaK salts were performed by using differential scanning calorimetry (DSC). Gold crucibles (TA Instruments, New Castle, DE) were used to contain salt samples for thermal analyses. Salt cells were prepared in a radiological glovebox that was maintained at <10 ppm

O_2 and <1 ppm H_2O. Crucibles were weighed, loaded with appropriate amounts of prepared salt, and hermetically sealed by using a mechanical press.

Phase transitions were measured by using a model STA 449C Jupiter® (NETZSCH Instruments North America, LLC, Burlington, MA) simultaneous thermal analyzer (STA). The STA is located on a marble slab within the glovebox to reduce vibrational interference. An ultra-high purity argon purge is used to maintain atmospheric conditions within the heated zone of the instrument during measurements. The temperature measurement of the instrument was calibrated by using five pure reference metals (Sn, Zn, Al, Ag, and Au) with melting points in the range of 231.9–1064 °C. Known amounts of different reference metals were placed in open alumina crucibles and heat flow measurements of each reference metal were performed over three heating cycles. The first cycle heated the sample at 20 °C min^{-1} to melt the reference metal and improve thermal contact between the metal and crucible. Two subsequent runs were performed to measure phase transitions at 5 °C min^{-1}. The 5 °C min^{-1} heating rate was selected as a compromise between the competing effects of thermal lag and instrument stability [3]. NETZSCH Proteus® software was used to determine the onset of melting for each reference metal. A quadratic fit was applied to the differences in measured and reference melting onsets and was used to calibrate heat flow measurements. Temperatures measured during DSC analyses are typically accurate to within 2 °C of actual values.

Thermal analyses of prepared salts were performed by loading a hermetically sealed gold crucible containing the salt sample onto the sample carrier of the instrument. The DSC was programmed to perform three heating cycles at the same heating rates used in the temperature calibration procedure. Prepared salt samples were heated and cooled over the ranges of 390–530 °C to ensure complete melting then solidification during each heating cycle. Three samples of each salt mixture were measured and NETZSCH Proteus® software was used to calculate transition temperatures.

3.2 Phase Transitions of Doped FLiNaK

Figure 1 shows the heat flow measurements during sequential runs at 5 °C min-1 (Ramp 1 and Ramp 2) performed with each of the three samples of the NiF_2 and CrF_3 doped FLiNaK salts. Measurements of FLiNaK provided under the interlaboratory salt study are included for comparison [ANL/CFCT-23/23]. Figures 1b, 1c, and 1d show expanded plots of heat flow measurements for FLiNaK, FLiNaK-CrF_3, and FLiNaK-NiF_2, respectively. The vertical dashed lines locate the averages of transition temperatures determined for multiple samples of each mixture. Calculated averages and three standard deviations (3 s) are reported for each doped salt mixture in Tables 12 and 13, respectively. Three standard deviations represents 99.7% of a normal distribution and bounds the full range of transition temperatures measured for the three samples.

Doped salts exhibit lower temperature features and reduced liquidus temperatures compared to the pure FLiNaK salt previously measured, which had a single transition with an onset at 454.9 °C and a liquidus temperature of 475.9 °C. The consistency of the transition temperatures measured in duplicate runs performed with the same sample indicate that measurement conditions were stable.

Consistency of the transition temperatures measured with different samples of the same doped salt mixture indicates the compositional uniformity of the salt mixtures. The range of values given by 3 s is within the 2 °C uncertainty of the DSC established by calibrations for all measured transition temperatures except the liquidus temperature for the FLiNaK-CrF_3. The variance in transition temperatures is attributed to minor composition differences in the three samples of FLiNaK-CrF_3.

The average measured transition temperature for the final onset of melting for FLiNaK-CrF_3, is within 2 °C of the average onset of melting of the previously measured FLiNaK without dopants (454.9 °C), while the final onset of melting for FLiNaK-NiF_2 salt is slightly lower at 452.3 °C. The differences in liquidus point between samples of FLiNaK salts with and without dopants are greater than the measurement uncertainty.

Table 12. Measured transition temperatures of FLiNaK-CrF_3 salt, in °C

Sample No.	Mass, mg	Ramp	Transition 1 Onset	Transition 2 Onset	Transition 3 Onset	Liquidus Endpoint
1	21.92	1	435.5	442.3	452.9	473.1
		2	435.2	442.6	452.9	472.6
2	22.19	1	435.4	441.3	453.5	471.2
		2	435.6	442.0	453.5	471.0
3	21.99	1	434.4	441.6	452.9	472.4
		2	434.6	442.3	452.8	472.8
FLiNaK-CrF_3		Average	435.1	442.0	453.1	472.2
		3 s	1.4	1.3	0.9	2.4

Table 13. Measured transition temperatures of FLiNaK-NiF_2 salt, in °C

Sample No.	Mass, mg	Ramp	Transition 1 Onset	Transition 2 Onset	Transition 3 Onset	Liquidus Endpoint
1	22.26	1	424.0	441.8	452.1	472.8
		2	424.2	441.3	452.1	473.3
2	22.03	1	424.9	441.1	452.3	472.1
		2	425.1	441.0	452.5	472.6
3	22.17	1	425.8	442.1	452.4	473.2
		2	424.6	442.1	452.2	473.5
FLiNaK-NiF_2		Average	424.8	441.6	452.3	472.9
		3 s	1.8	0.5	0.2	1.4

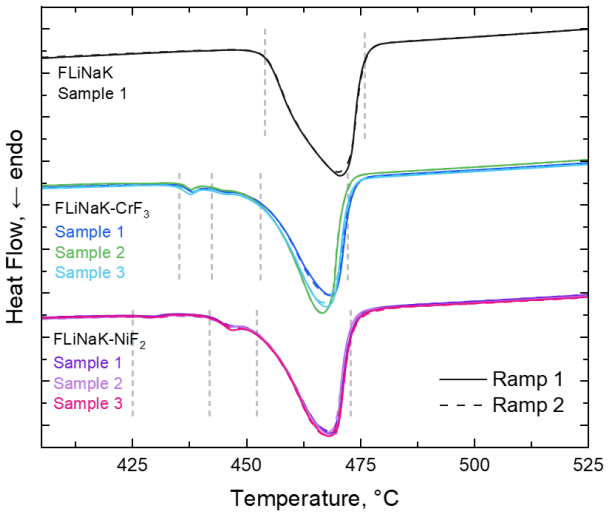

(a)

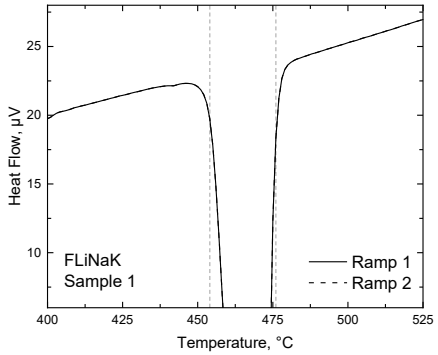

(b)

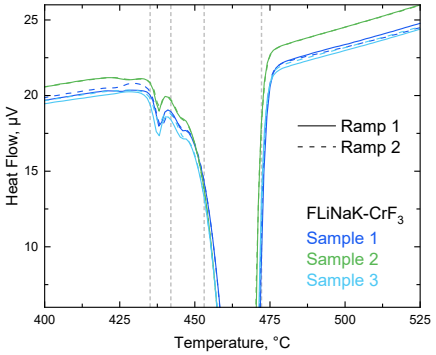

(c)

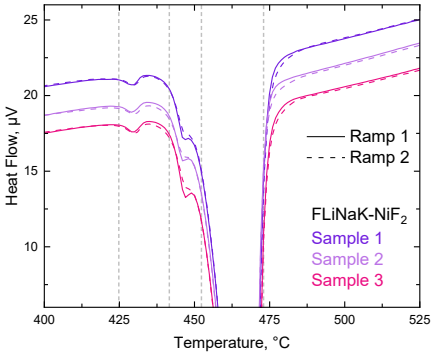

(d)

Figure 1. DSC responses of (a) FLiNaK, FLiNaK-CrF_3, and FLiNaK-NiF_2 salt and expanded plots of (b) FLiNaK, (c) FLiNaK-CrF_3, and (d) FLiNaK-NiF_2 responses showing onsets of phase transitions.

Figure 2 shows the heat flow measurements during sequential runs at 5 °C min^{-1} (Ramp 1 and Ramp 2) performed with each of the three samples of doped salt mixtures, FLiNaK-UF_4-A, and FLiNaK-UF_4-B, compared with previous measurements of FLiNaK provided under the inter-laboratory salt study for comparison. Figures 2b–2c and 2d –2e, show expanded plots of heat flow measurements for FLiNaK-UF_4-A and FLiNaK-UF_4-B respectively. The vertical dashed lines locate the averages of transition temperatures determined for multiple samples of each mixture. Calculated averages and three standard deviations (3 s) are reported for each doped salt mixture in Tables 14 and 15, respectively.

The additions of ~ 12 wt. % UF_4 with different concentrations of dissolved oxygen resulted in additional low-temperature and high-temperature features and a decrease in the average onset of the melting peak compared to those for FLiNaK. Shoulder features were also observed in measurements of FLiNaK-UF_4-A and FLiNaK-UF_4-B at 512.9 °C and 510.5 °C, respectively, indicating increases in melting endpoint temperature compared to the liquidus endpoint of FLiNaK (472.9 °C). Changes in phase equilibria are expected when adding a significant amount of a major constituent, in this case UF_4 containing dissolved oxygen.

Differences in the measured onset of Transition 2, the melting endpoint, and Transition 4 in duplicate runs performed with the same samples of FLiNaK-UF_4-A and FLiNaK-UF_4-B indicate that measurements were affected by instability in measurement conditions. The range of values given by 3 s for Transition 1 and the melting endpoint temperature of both FLiNaK-UF_4-A and FLiNaK-UF_4-B are greater than the 2 °C uncertainty of the DSC. This indicates compositional non-uniformity across samples of the same salt for salt mixtures FLiNaK-UF_4-A and FLiNaK-UF_4-B. This is a limitation of taking small samples of a multi-component mixture where one of the components is present in trace amounts (e.g. UO_2) and is likely to be distributed non-uniformly.

Differences in the average measured onsets of Transitions 1 and 2 for FLiNaK-UF_4-A and -B are within the measurement uncertainty while the onsets of Transition 3 and the melting endpoints differ by 2.8 °C and 3.0 °C, respectively. Any differences in thermal behavior of FLiNaK-UF4 -A and -B due to the difference in dissolved oxygen content cannot be distinguished from the measurement uncertainty.

Table 14. Measured transition temperatures of FLiNaK-UF_4-A salt, in °C

Sample No.	Mass, mg	Ramp	Transition 1 Onset	Transition 2 Onset	Transition 3 Onset	Melting Endpoint	Transition 4 Onset
1	22.26	1	422.8	428.0	445.0	512.7	558.5
		2	423.0	—	444.6	513.2	558.7
2	22.03	1	419.8	426.5	444.9	513.7	531.2
		2	422.8	—	444.8	513.4	531.2
3	22.17	1	421.6	427.7	444.1	513.5	531
		2	421.0	428.0	444.7	510.6	530.9
FLiNaK-UF_4-1		Average	421.8	427.5	444.7	512.9	540.3
		3 s	3.5	1.8	0.9	3.2	13.0

Table 15. Measured transition temperatures of FLiNaK-UF_4-B salt, in °C

Sample No.	Mass, mg	Ramp	Transition 1 Onset	Transition 2 Onset	Transition 3 Onset	Melting Endpoint	Transition 4 Onset
1	21.92	1	421.6	427.0	442.4	513.5	530.5
		2	420.3	—	442.1	506.8	557.5
2	22.19	1	420.8	426.8	441.3	513.9	531.6
		2	418.3	—	441.9	510.9	531.0
3	21.99	1	420	426.9	441.7	512.6	531.0
		2	419.4	—	442.2	505.3	530.7
FLiNaK-UF_4-1		Average	421.8	420.1	426.9	510.5	535.4
		3 s	3.1	0.2	1.1	9.9	9.9

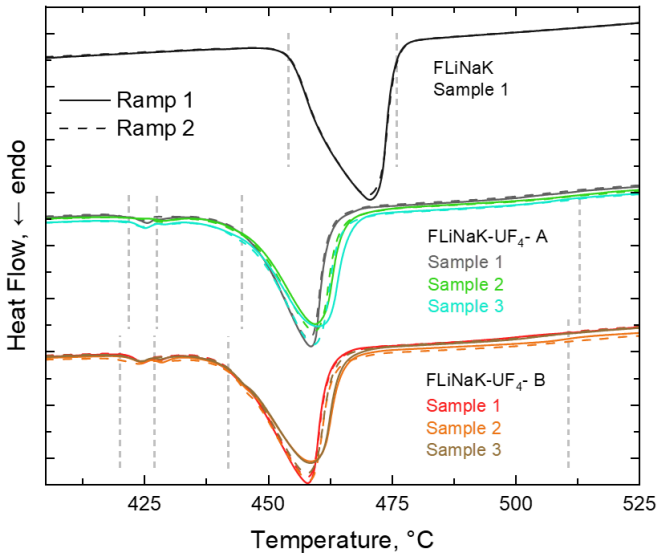

(a)

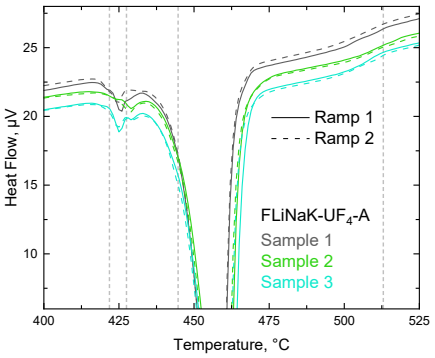

(b)

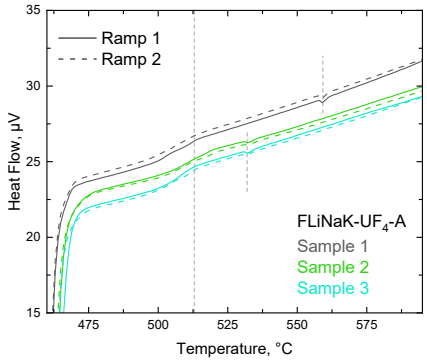

(c)

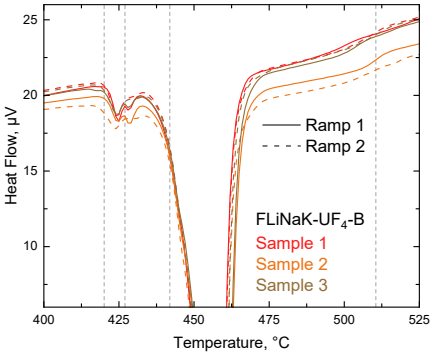

(d)

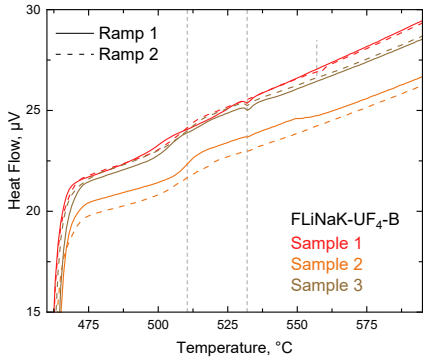

(e)

Figure 2. DSC responses of (a) FLiNaK, FLiNaK-UF_4-A, and FLiNaK-UF_4-B salt and expanded plots of (b–c) FLiNaK-UF_4-A and (d–e) FLiNaK-UF_4-B responses showing onsets of phase transitions.

4. Specific Heat Capacity

4.1 Differential Scanning Calorimetry

Specific heat capacities of corrosion product-doped FLiNaK salts were determined from traditional DSC analyses of empty gold crucibles, a sapphire reference material, and salt samples by using the ratio method [4]. Salt samples that were prepared for thermal analyses were also used for specific heat capacity measurements. A NETZSCH model 449C Jupiter STA was used to perform heat flow measurements of different samples.

The calculation of heat capacity is based on measurements of three different materials: salt, sapphire, and an empty gold cell. Heat flow through an empty gold crucible is first measured to establish a baseline that represents instrumental response under the conditions of the measurement. The baseline heat flow is subtracted from heat flows measured in subsequent analyses of the sapphire reference material and salt sample. The three measurements were performed on the same day to minimize experimental drift due to variation in the environmental conditions over time (e.g., glovebox pressure, temperature, and oxygen and moisture concentrations). The positions of crucibles on the sample carrier were the same in each series of measurements to maintain consistent heat flow paths in each series of three measurements. Also, no other work was done in the laboratory while specific heat capacity measurements were performed.

Identical heating cycles were used in the three sequential measurements. The sample was first heated at 20 °C min^{-1} to a specified temperature T_1 that is higher than the melting point of the salt sample. A 15-minute isothermal hold was then performed to stabilize the system at T_1. Following the equilibration step, the material was heated at 10 °C min^{-1} to a higher temperature T_2 and then isothermally held at T_2 for 15 minutes before cooling to room temperature. The background-subtracted heat flows measured for sapphire and salt were manually adjusted to a common zero using the values determined during the low-temperature and high-temperature isothermal holds [5]. Measurements with samples of FLiNaK-CrF_3, FLiNaK-NiF_2, and FLiNaK-UF_4-A and -B were performed over the temperature range of 520–730 °C, 500–730 °C, and 500–730 °C, respectively.

The specific heat capacity of the salt sample, C_p^s, is calculated by using Equation 1 [6], where m_r and m_s are the masses of the sapphire reference material and salt sample, respectively, m_{cr}^r and m_{cr}^s are the masses of the gold crucibles that contain the sapphire and salt sample, $\Delta\varphi_r$ and $\Delta\varphi_s$ are the baseline-corrected and zero-adjusted heat flow values measured for the sapphire and salt sample, and C_{p}^s, C_{p}^r and C_{p}^{cr} are the heat capacity values of the salt sample, sapphire, and gold crucible, respectively.

$$C_{\mathrm{p}}^s = \frac{m_r}{m_s}\frac{\Delta\varphi_s}{\Delta\varphi_r}C_p^r + \frac{m_{cr}^r - m_{cr}^s}{m_s}C_p^{cr} \ . \qquad (1)$$

The first term in Equation 1 represents the conventional ratio method, which represents the energy balance between heat flow measurements of the sapphire standard and the salt samples. The second term is a correction that takes differences in mass between the gold crucibles used to contain the sapphire and salt samples into account. The weights of the sapphire and salt samples and crucibles were matched to improve uniformity between measurements. The heat flow measured for the sapphire and salt samples were automatically corrected by the instrument software by subtracting the baseline heat flow measured using two empty crucibles. The same baseline was used for background correction of measurements with sapphire and salt. Salt samples were weight-matched to the sapphire sample to within 1% and crucible weights were matched to within 1.5%. The heat capacities of sapphire and gold reported by Ditmars et al. [7] and Arblaster [8], respectively, were used in calculations of specific heat capacity.

4.2 Specific Heat Capacity of Doped FLiNaK by DSC

Specific heat capacities of doped FLiNaK are shown in Figure 3. Horizontal black lines locate the average and three standard deviation values of specific heat capacities determined previously for FLiNaK [1], which is 1.79 ± 0.18 J g^{-1} K^{-1}. Specific heat capacity values were not calculated at temperatures corresponding to phase transitions, at which specific heat capacity is undefined. Gaps in curves for FLiNaK-UF_4-A and FLiNaK-UF_4-B occur in these regions. Phase transitions occurring at different temperatures for different samples of the same salt mixture provide additional evidence of compositional non-uniformity in both FLiNaK-UF_4 salt mixtures. Heat capacity values for FLiNaK-CrF_3, FLiNaK-NiF_2, FLiNaK-UF_4-A, and FLiNaK-UF_4-B were in the range of 1.45–1.91, 2.16–2.43, 1.87–2.41, and 1.71–2.01 J g^{-1} K^{-1}, respectively.

No trends in the temperature dependance of specific heat capacity for different doped FLiNaK salt mixtures occur over this temperature range exceeding the measurement uncertainty for each salt mixture, which is reported as three standard deviations of the measured values. Three standard deviations represents 99.7% of a normal distribution and bounds the full range of values measured for the three samples. Differences in average specific heat capacity between measurements of FLiNaK and doped salt mixtures are within the uncertainty of the measurements except for the difference between FLiNaK and FLiNaK-NiF_2 measurements, which are greater than the measurement uncertainty. The presence of low concentrations of NiF_2 increases the specific heat capacity of molten FLiNaK over this temperature range. Sources of uncertainty in heat capacity measurements include variation in crucible placement and changes in glovebox pressure during measurements.

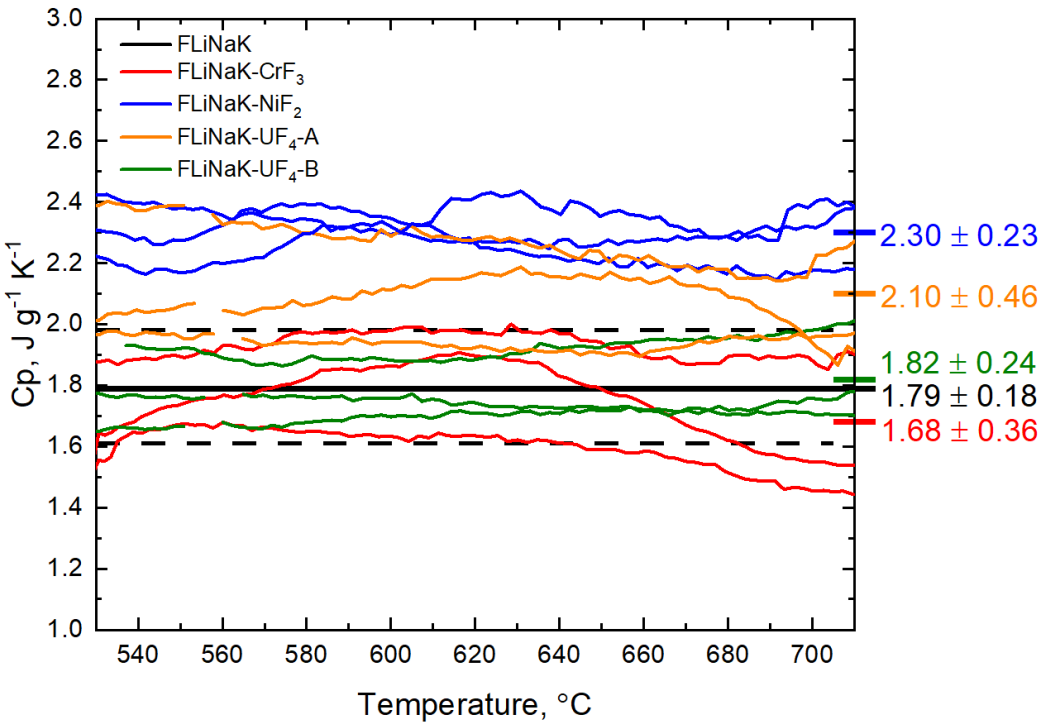

Figure 3. Heat capacity values of FLiNaK [1], FLiNaK-CrF_3, FLiNaK-NiF_2, FLiNaK-UF_4-A, and FLiNaK-UF_4-B measured by using traditional DSC. Solid and dashed horizontal lines locate the average and 3s heat capacity values, respectively, for FLiNaK.

4.3 Modulated Differential Scanning Calorimetry

Specific heat capacity measurements of sapphire and molten FLiNaK salt were performed by using modulated differential scanning calorimetry (MDSC) for comparison to values determined by using traditional DSC. Modulated DSC requires less time to obtain specific heat capacity measurements compared to traditional DSC and exhibits lower sensitivity to changes in lab environment. The MDSC method [9] is performed by adding a sinusoidal temperature oscillation to a linear heating rate. Salt samples in gold cells that had been used in previous specific heat capacity measurements made by traditional DSC [1] were used for MDSC measurements. Modulated heat flow measurements were performed by using an SDT 650 model simultaneous differential scanning calorimeter-thermogravimetric analyzer (DSC-TGA – TA Instruments, New Castle, DE) within an argon atmosphere glovebox that maintained an environment with <10 ppm O_2 and <5 ppm H_2O. All measurements were performed with an ultra-high purity argon purge gas flowing through the heated zone at 200 ml min^{-1} for the duration of each test.

The specific heat capacity is calculated by using Equation 2, where A_{ϕ_p} is the amplitude of the periodic heat flow, ω is the frequency of the periodic heating rate, T_A is the temperature amplitude, and K is a calibration factor obtained from a heat flow calibration measurement of a sapphire

reference. TA Instruments TRIOS® software was used to analyze measured heat flows and calculate specific heat capacities [6].

$$C_P = \frac{A_{\phi_p}}{T_A \omega} K \tag{2}$$

Figure 4 shows heat flow calibration runs performed to measure the specific heat capacity of a sapphire sample encapsulated in a hermetically sealed gold cell. Measured and reference values were compared, and a calibration factor K was calculated over the range of measured temperatures. This calibration factor was used to correct subsequent heat flow measurements of salt samples performed on the same day with identical experimental parameters (e.g., temperature range, heating rate, amplitude and modulation period).

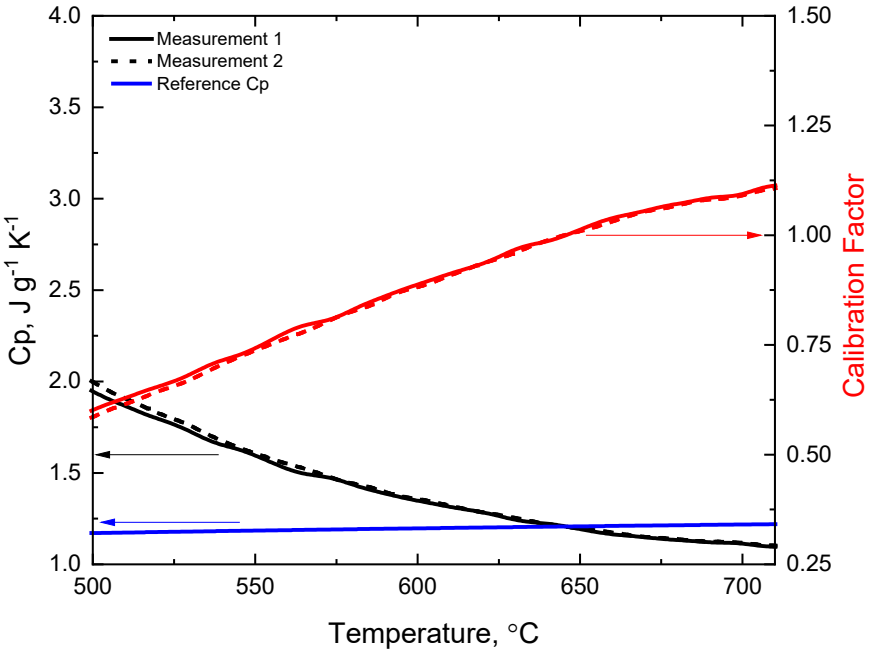

Figure 4. Measured and reference specific heat capacity values of a sapphire sample used to calculate heat flow calibration factors.

The temperature response of the DSC-TGA used for MDSC heat capacity measurements was calibrated by using the same procedure developed for temperature calibration of the NETZSCH® DSC performing thermal analyses of five pure reference metals (Sn, Zn, Al, Ag, and Au). Known amounts of different reference metals were placed in open alumina crucibles and heat flow measurements of each reference metal were performed over two heating cycles. The first cycle heated the sample at 20 °C min^{-1} to melt the reference metal and improve thermal contact between the metal

and crucible. The second run was performed to measure phase transitions at 5 °C min^{-1}. TA instruments TRIOS® software was used to measure the onset of melting for each reference metal. A quadratic fit was applied to differences in measured and reference melting onsets and used to calibrate the temperature in subsequent heat flow measurements. The calibration curve is plotted in Figure 5 as ΔT = nominal – measured with a quadratic regression curve generated within the instrument software. The double-headed arrows show the residuals for data points used in the regression. Adjustment of the measured temperatures using the calibration curve provides temperatures that are accurate to within 2 °C across this temperature range based on results for each reference metal. These results are similar to calibrations of the DSC prior to heat capacity measurements [1].

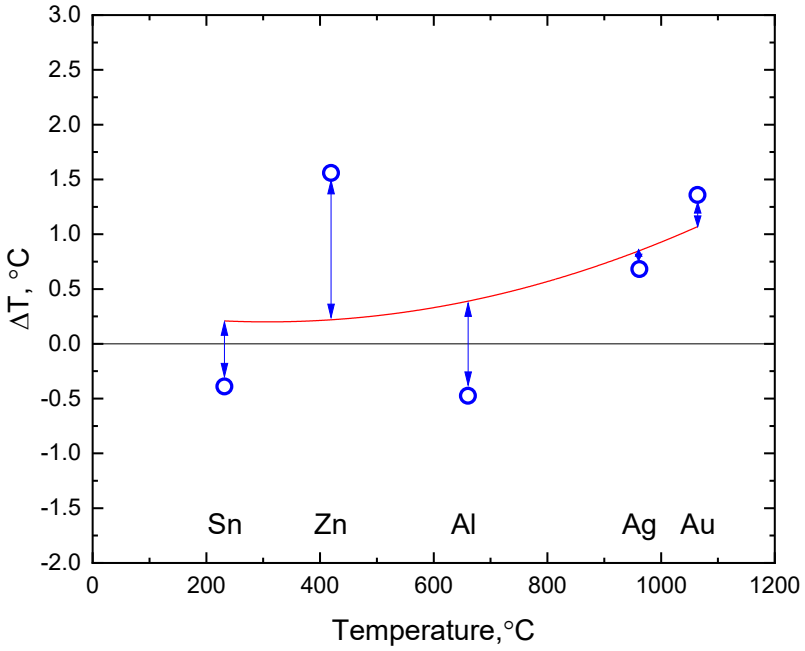

Figure 5. Temperature calibration results showing differences between measured and nominal melting temperatures of five reference metals with the regression curve

4.4 Specific Heat Capacity by Modulated Differential Scanning Calorimetry

The specific heat capacity of sapphire was first measured to confirm the effectiveness of the instrument calibrations by performing both the first and second measurements on the same sapphire sample. Measurements of the sapphire sample consisted of a 20 °C min^{-1} ramp to 500 °C, a 16-minute modulated isothermal hold (with amplitude of 1 °C and a modulation period of 120 s), and a modulated heating ramp at 3 °C min^{-1} to 680 °C (with the same modulation conditions). The measured specific heat

capacities of sapphire are shown in Figure 6. Values of the two measurements of the heat capacity of sapphire over this temperature range (red curves) were both in the range of 1.17–1.23 J g^{-1} K^{-1}, whereas values of the sapphire reference (black curve) increased from 1.17 to 1.21 J g^{-1} K^{-1} over this range [7]. All measured values of sapphire were within ±0.05 J g^{-1} K^{-1} of the reference value at the same temperature. The temperature dependence of the measured data matches that of the sapphire reference material. Uncertainty analysis and the effects of instrument stability, heating parameters, and analysis of heat flow data generated by MDSC on derived specific heat capacity are the focus of active research.

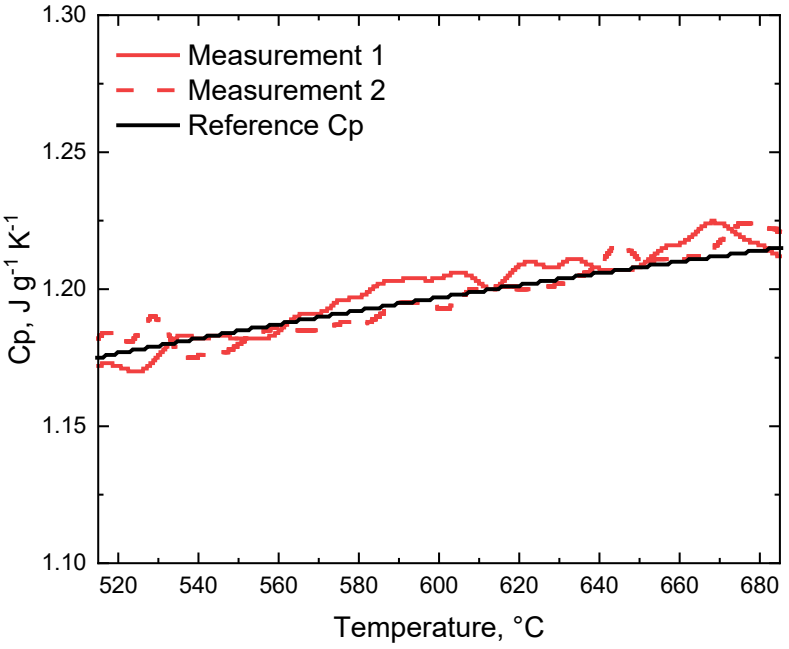

Figure 6. Heat capacities of sapphire measured by MDSC compared to the reference value.

Measured specific heat capacities of FLiNaK provided under the interlaboratory salt study by using traditional DSC and MDSC are compared in Figure 7. Heat capacities measured by MDSC show a slightly positive temperature dependence while measurements performed by traditional DSC are flat or show slightly negative temperature dependence. The average heat capacity of FLiNaK determined by MDSC over the range of temperatures (two samples) is 2.25 ± 0.13 J g^{-1} K^{-1} while that determined using the ratio method is 1.79 ± 0.18 J g^{-1} K^{-1} with uncertainties reported as three standard deviations of the measured values. Three standard deviations represents 99.7% of a normal distribution and bounds the full range of values measured for the three samples. Differences in the heat capacity values for FLiNaK samples measured by using DSC and MDSC and possible bias might be attributable to differences in instrument heat flow calibration procedures, glovebox conditions (the DSC and MDSC instruments are housed in different gloveboxes), and heating parameters. Both operational effects and the analysis of heat flow data generated by MDSC on derived specific heat capacity are the focus of active research.

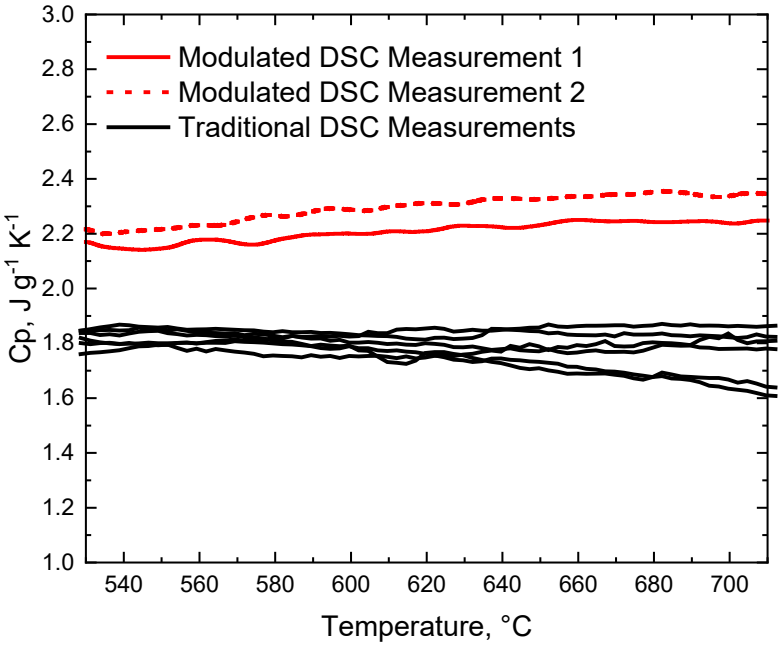

Figure 7. Heat capacity values of FLiNaK measured by using traditional and modulated DSC.

5. Conclusion

Phase transitions of FLiNaK salt mixtures with corrosion product dopants were measured by using DSC and specific heat capacity was measured by using traditional DSC and MDSC. Additional low-temperature and high-temperature transitions were detected in measurements with samples of doped FLiNaK salts compared to previous measurements of FLiNaK. The addition of CrF_3 and NiF_2 resulted in lower onset of melting temperatures and melting endpoint temperatures compared to values measured for FLiNaK and additions of UF_4 containing dissolved oxygen resulted in higher melting endpoint temperatures. The variance in measured transition temperatures for samples of FLiNaK-CrF_3, FLiNaK-UF_4-A, and FLiNaK-UF_4-B is attributed to minor compositional differences in the three samples of each mixture. The effects of CrF_3, NiF_2, and UF_4 at these concentrations exceed the DSC measurement uncertainty for the majority of measured transitions. No trends in temperature dependency of specific heat capacity data can be discerned because differences in average values for measurements of FLiNaK-CrF_3, FLiNaK-UF_4-A, and FLiNaK-UF_4-B are within the measurement uncertainty determined for FLiNaK. The difference in average specific heat capacity of FLiNaK-NiF_2 and FLiNaK is greater than the measurement uncertainty. The use of modulated DSC (MDSC) to measure specific heat capacities of sapphire and molten salts is being assessed. The MDSC method requires shorter durations and is expected to be less sensitive to instabilities in the glovebox environment. The magnitude and temperature dependence of specific heat capacity values for sapphire measured by using MDSC were in good agreement with reference values. However, differences of 0.4–0.7 J g^{-1} K^{-1} were observed between measurements of FLiNaK performed with traditional DSC and MDSC over the temperature range 500–680 °C, which indicates bias in one or both methods. Effects of heat flow calibration procedures and heating parameters used for MDSC are the focus of active research to assess the accuracy of each method.

References

[1] M.A. Rose, L.D. Gardner, and T.T. Lichtenstein, Property Measurements of NaCl-UCl_3 and LiF-NaF-KF Molten Salts Doped with Surrogate Fission Products, ANL/CFCT-23/23, Argonne National Laboratory (2023).

[2] L.D. Gardner, K.A. Chamberlain, and M.A. Rose, Property Measurements of LiF-NaF-KF Molten Salts Doped with Surrogate Fission Products, ANL/CFCT-24/23, Argonne National Laboratory (2024).

[3] L.D. Gardner and M.A. Rose, Uncertainty Analyses of Molten Salt Property Measurements, ANL/CFCT-25/5, Argonne National Laboratory, (2025).

[4] American Society for Testing and Materials, E1269-01 Standard Test Method for Determining Specific Heat Capacity by Differential Scanning Calorimetry (2001) E 1269-01, https://doi.org/10.1520/E1269-11R18.

[5] T. Lichtenstein, M.A. Rose, J. Krueger, E. Wu, and M.A. Williamson, Thermochemical Property Measurements of FLiNaK and FLiBe in FY 2020, ANL/CFCT-20/37 Rev. 1, Argonne National Laboratory (2020).

[6] G.W.H. Höhne, W.F. Hemminger, H.-J. Flammersheim (2003). Differential Scanning Calorimetry, 2nd ed., Springer, New York, NY.

[7] D.A. Ditmars, S. Ishihara, S.S. Chang, G. Bernstein, and E.D. West, Enthalpy and Heat Capacity Standard Reference Material: Synthetic Sapphire (α-Al_2O_3) From 10 to 2250 K, *J. Res. Natl. Bur. Stand.*, 87, 2, 159–163 (1982), https://doi.org/10.6028/jres.087.012.

[8] J.W. Arblaster, Thermodynamic Properties of Gold, *J. Phase Equilibria Diffus.*, 37, 229–245 (2016), https://doi.org/10.1007/s11669-016-0449-z.

[9] American Society for Testing and Materials, E2716-09 Standard Test Method for Determining Specific Heat Capacity by Sinusoidal Modulated Temperature Differential Scanning Calorimetry (2014) E 2716-09, https://doi.org/10.1520/E2716-09R14.

Chemical and Fuel Cycle Technologies Division
Argonne National Laboratory
9700 South Cass Avenue, Bldg. 205
Lemont, IL 60439

www.anl.gov

Argonne National Laboratory is a U.S. Department of Energy laboratory managed by UChicago Argonne, LLC